NASA Technical Memorandum 104529

Ultrasonic Evaluation of Oxidation and Reduction Effects on the Elastic Behavior and Global Microstructure of $YBa_2Cu_3O_{7-x}$

Don J. Roth
Lewis Research Center
Cleveland, Ohio

Mark R. DeGuire
Case Western Reserve University
Cleveland, Ohio

and

Leonard E. Dolhert
W.R.Grace & Company
Columbia, Maryland

July 1991

NASA

ULTRASONIC EVALUATION OF OXIDATION AND REDUCTION EFFECTS ON THE ELASTIC BEHAVIOR AND GLOBAL MICROSTRUCTURE OF $YBa_2Cu_3O_{7-x}$

Don J. Roth
National Aeronautics and Space Administration
Lewis Research Center
Cleveland, Ohio 44135

Mark R. DeGuire
Dept. Materials Science and Engineering
Case Western Reserve University
Cleveland, Ohio 44106

and

Leonard E. Dolhert
W.R. Grace & Co.
Research Division
Columbia, Maryland 21044

I. ABSTRACT

Ultrasonic velocity measurement techniques were used to evaluate the effects of oxidation and reduction on the elastic properties, global microstructure and oxygen content of the $YBa_2Cu_3O_{7-x}$ ceramic superconductor for samples ranging from 70 to 90 percent of theoretical density. Bulk density, velocity and elastic modulus generally increased with increasing oxygen content upon oxidation, and this behavior was reversible. Velocity image patterns were similar after oxidation and reduction treatments for a 90 percent dense sample, although the velocity value at any given point on the sample was changed following the treatments. The unchanging pattern correlated with destructive measurements showing that the spatial pore distribution (fraction and size) was not measureably altered after the treatments. Changes in superconducting behavior, crystal structure, and grain structure were observed consistent with changes in oxygen content.

II. INTRODUCTION

The last several years have seen the remarkable development of a new class of ceramics exhibiting superconductivity to unprecedentedly high temperatures.[1,2,3,4] The subject of this study is the $YBa_2Cu_3O_{7-x}$ (YBCO) superconductor. Oxidation is the final and arguably the most important processing step in the manufacture of YBCO.[5,6,7] This step results in an increase in oxygen content from the sintered state, making the material superconducting. Loss of oxygen (reduction) can cause diminishment or loss of superconductivity.[8]

In this study, we consider several aspects concerning the effects of oxidation and reduction on YBCO. First, elastic modulus change resulting from oxidation and

reduction is investigated. Changes in the mechanical (as well as the superconductor) behavior of YBCO with oxygen content changes are of concern for applications such as high field magnets which experience large loads.[9] Second, global microstructural change upon oxidation and reduction is studied. Global microstructural evolution is of interest as microstructure plays a large role in YBCO superconducting behavior.[10] Finally, the use of ultrasonic velocity techniques to noninvasively monitor oxidation and reduction processes is evaluated. The use of noninvasive techniques for process control are desirable for their potential time and cost savings.[11]

III. BACKGROUND

A. Ultrasonic Velocity, Elastic Modulus, and Material Change

When there are no boundary effects present, the velocity (V) of a longitudinal elastic wave in a bulk solid is determined from the elastic modulus (E), density (ρ), and Poisson's ratio (ν) of the solid according to[12]

$$V=\left[\frac{E(1-\nu)}{\rho(1+\nu)(1-2\nu)}\right]^{1/2} \qquad (1)$$

In theory, any (compositional and/or structural) change that affects the E, ρ, or ν of the crystals composing the solid should affect the ultrasonic velocity of high-frequency stress waves, i.e., velocity is sensitive to changes in density and elastic strain state (dynamic or static) of crystals.[13,14] Additionally, if the material is porous, any change in the amount of porosity that causes changes in bulk density and (apparent) elastic properties[15] of the material will strongly affect velocity.[16] In practice, ultrasonic velocity is an extremely sensitive measure of material change; it is estimated that velocity differences on the order of 0.00001 % can be detected under the best experimental conditions.[13] Equation (1) can be rearranged to show that E is proportional to ρV^2.

Ultrasonic studies have been used previously to nondestructively determine oxygen content changes in metal alloys,[17,18] evaluate the effect of oxygen content on elastic properties of metal alloys,[17] and examine spatial variations in microstructure.[10,19,20,21,22,23] It was reported that longitudinal wave velocity increased with an increase in oxygen content for titanium-oxygen alloy[17] while velocity decreased with increasing oxygen content for titanium-6211 alloy.[18] In both of these studies, a bulk density increase accompanied the oxygen content increase. A decrease in velocity with increasing density as seen in reference 18 is contrary to all of the empirical data presented in reference 16, and suggests that other effects of oxidation besides density change (such as accompanying compositional changes and structural transformations) may significantly influence velocity. References 19, 20 and 21 examined spatial variations in microstructure for structural ceramics using ultrasonic velocity measurements. Reference 10 determined that ultrasonic velocity variations across a YBCO sample were likely to be caused by spatial variations in volume percent porosity.

B. Structural Changes in YBCO With Changes in Oxygen Content

$YBa_2Cu_3O_{7-x}$ in its optimum superconducting form (normal-to-superconducting transition temperature, T_c = 90 K) has an orthorhombic crystal structure with (7-x) = 6.8 to 7.0.[6,7] If (7-x) ≈ 6.0 to 6.4, YBCO is tetragonal with semiconducting electrical behavior.[24] Additional YBCO structures reported include the orthorhombic II (OII) and tetragonal T′ phase. The OII phase is characterized by (7-x) ≈ 6.5 - 6.8[25] and diminished T_c (e.g., $YBa_2Cu_3O_{6.56}$ with T_c about 60 K[6,26]). The tetragonal T′ phase is characterized by (7-x) > 7, and semiconducting behavior.[27,28,29]

Changes in $YBa_2Cu_3O_{7-x}$ oxygen content are accommodated primarily by changes in the oxygen atom occupancy on the basal planes.[7] As oxygen content increases, the c-axis and b-axis contract while the a-axis of the unit cell expands, and oxygen vacancy ordering takes place along the a-axis.[30] The cell volume for tetragonal $YBa_2Cu_3O_6$ is 176.20 Å^3 and its cell density is 6.125 g/cm^3. The cell volume for orthorhombic $YBa_2Cu_3O_7$ is 173.30 Å^3 and its cell density is 6.381 g/cm^3. Thus, the tetragonal to orthorhombic structure transformation where (7-x) increases from 6.0 to 7.0 will result in a 1.6% volume decrease and a 4% density increase. Twinning within grains of polycrystalline YBCO normally accompanies the structural transformation from tetragonal to orthorhombic to relieve the induced shear stresses.[31] Thus, during the oxidation and reduction of YBCO, oxygen vacancy ordering, crystal structure, grain structure (twinning) and crystal density are changed. These changes will likely affect stress wave velocity in YBCO crystals.

Changes in the bulk YBCO material also may result from oxidation and reduction. Depending on the oxidation/reduction peak temperature, the material may sinter resulting in pore distribution (fraction and size) changes. Furthermore, cracking in YBCO can result from residual stresses induced by 1) differential contraction of the c-axis relative to the a- and b-axes during structural transformation from tetragonal to orthorhombic, 2) axial thermal contraction anisotropy of YBCO grains upon cooling and/or 3) contraction anisotropy (simple and/or thermal) between an oxygenated surface and incompletely-oxygenated bulk upon cooling.[7] The latter cause of macrocracking is especially prevalent in higher (≥ 90%) density YBCO samples. Such changes in the bulk during oxidation and reduction are also likely to affect velocity, and possibly result in velocity changes from region to region within the bulk if microstructural changes are not uniform.

IV. EXPERIMENTAL

A. Specimens

Five YBCO disk-shaped samples (labeled 1, 2, 3, 4 and 5) were manufactured from one batch of starting powder. YBCO powder for the samples was made by first dissolving the appropriate amount of metal nitrates in water, and then coprecipitating a hydroxy-carbonate by mixing aqueous tetramethylammonium carbonate with the aqueous nitrate solution. The precipitate was then filtered and dried. The dried solids were precalcined in air at 540 °C for 5 hours to remove organic matter, and then calcined in flowing air at 880 °C for 50 hours followed by cooling to 300 °C over 16 hours. At 600 °C,

flowing air was shut off and replaced by flowing oxygen.

The YBCO powder was ball-milled for 1.5 hours in a polyurethane-lined jar mill with highly wear-resistant yttria-stabilized zirconia balls. The powder and balls were separated by shaking them in a stainless-steel 100-mesh sieve. Jar loading and unloading, and sieving were done in a low-CO_2/low-H_2O glovebox. This procedure produced a powder with a broad size distribution; average particle size was about 1.5 μm with no particles greater than 45 μm.

Disks approximately 25.4 mm diameter by 6.3 mm thick were made by die-pressing at 5000 psi followed by cold isostatic-pressing at 20,000 psi for 5 minutes. The sample disks were sintered and cooled while sitting on 20-mesh MgO single crystals in a 7 cm diameter tube furnace in flowing gas (ultra-high purity oxygen or argon (flow rate = 200 - 240 cm^3/min)). Disks 2, 3 and 4 first experienced the sintering/cooling oxidation schedule of table I(a) (page 5) while samples 1 and 5 first experienced the sintering/cooling nonoxidation of schedule of table I(b).

The peak sintering temperature (in the schedules of tables I(a) and I(b)) for sample disks 1 - 5 was changed to obtain a range of bulk densities. Samples 1, 2, 3, 4 and 5 had peak sintering temperatures of 937, 947, 954, 966, and 976 °C ($\pm$ 2 °C), resulting in bulk densities of 4.37, 4.99, 5.06, 5.78 and 5.74 ($\pm$ 0.03) g/cm^3, respectively, spanning a range of approximately 68 to 92 % of theoretical density. Bulk density was determined from sample mass and dimensions. The samples were dry cut into two thinner disks 3 mm thick using a slitting saw with a 180 grit diamond-impregnated steel blade. In preparation for ultrasonic measurements, one of the 3 mm thick disks from each sample (except sample 5) was cut into two semicircular halves. In preparation for a.c. susceptibility measurements, a bar of approximate dimensions 10 mm by 3 mm by 2 mm was dry cut from both edge and center regions of the 3 mm thick circular disk from samples 1 - 4. For sample 5, one bar was cut from one of the 3 mm thick circular disks. The bars, semi-circular sections, and intact sample 5 circular disk were dry machined on a surface grinder using 150 and 320 grit diamond wheels while removing a minimum of material. Resulting parallel surfaces of the bars and semi-circular sections were flat and parallel to $\pm$ 0.010 mm. The sample 5 machined circular disk had top and bottom surfaces flat and parallel to $\pm$ 0.002 mm.

To study the effects of oxidation and reduction on elastic properties and microstructure, the pieces cut from initially-oxidized samples (2, 3, and 4) were reduced in argon (table I(c)), the pieces cut from initially-unoxidized samples (1 and 5) were oxidized (table I(d)), and the pieces cut from sample 5 were oxidized again for an extended time (table I(e)), and finally reduced in argon (table I(c)).

B. Ultrasonics

1. Pulse-echo Velocity Measurement

The pulse-echo contact technique (figures 1(a) and (b)) (page 7) was used to obtain ultrasonic waveform data.[32,33] In this technique, an ultrasonic pulse generated by a piezoelectric

Tables I(a)-(e). Heating/Sintering/Cooling Schedules for YBCO Samples

Table I(a). Sinter and Cool in Oxygen for Samples 2, 3, and 4

Segment	Heat to: (temp,°C)	Cool to: (temp,°C)	Ramp period: (time,hrs.)	Atmosphere
1	100		0.167	oxygen
2	peak[a]		4.5	oxygen
3	peak hold		1.5	oxygen
4		600	2	oxygen
5		300	13	oxygen
6		200	1	oxygen
7		25	9	oxygen

[a]peak sintering temperature for samples 2, 3 and 4 = 947, 954 and 966 °C, ±2 °C, respectively

Table I(b). Sinter in Oxygen and Then Cool in Argon for Samples 1 and 5

Segment	Heat to (temp, °C)	Cool to: (temp, °C)	Ramp period: (time, hrs.)	Atmosphere
1	100		0.167	oxygen
2	peak[a]		4.5	oxygen
3	peak hold		1.5	oxygen
4		825	0.75	oxygen
5		hold at 825	2	oxygen → argon
6		600	1.25	Argon
7		300	13	Argon
8		200	1	Argon
9		25	9	Argon

[a]peak sintering temperature for samples 1 and 5 = 937 and 976 °C, ±2 °C, respectively

Table I(c). Reduction For YBCO samples 2, 3, 4, and 5

Segment	Heat to: (temp, °C)	Cool to: (temp, °C)	Ramp period: (time, hrs.)	Atmosphere
1	100		0.167	oxygen
2	800		4	oxygen
3	hold at 800		7	oxygen → argon
4		600	1.25	argon
5		300	13	argon
6		200	1	argon
7		25	9	argon

Table I(d). Oxidation For YBCO samples 1 and 5

Segment	Heat to: (temp, °C)	Cool to: (temp, °C)	Ramp period: (time, hrs.)	Atmosphere[a]
1	100		0.167	argon
2	825		4.5	argon
3	hold at 825		2	argon → oxygen
4		600	1.25	oxygen
5		300	13	oxygen
6		200	1	oxygen
7		25	9	oxygen

[a]Argon was flushed through the furnace for 2 hours prior to the run

Table I(e). Extended Oxidation For YBCO sample 5

Segment	Heat to: (temp, °C)	Cool to: (temp, °C)	Ramp period: (time, hrs.)	Atmosphere
1	100		0.167	oxygen
2	825		4.5	oxygen
3		600	1.25	oxygen
4		hold at 600	53[a]	oxygen
5		300	13	oxygen
6		200	1	oxygen
7		25	9	oxygen

[a]Power outage occurred 45 hours into 48 hour hold; the schedule was started over and another 8 hour hold took place

crystal is propagated into a buffer rod-couplant-sample (BCS)configuration. The ultrasound reflects off the front and back surfaces of the sample and travels back to the crystal. A pulser-receiver was used to electrically pulse the crystal and receive the pulses reflected from the sample. The received pulses were digitized into 512 point arrays at a sampling rate of 0.512 - 1.024 GHz. Each pulse was acquired 64 times and an average was obtained. The time delay (τ) between the back-surface-reflected pulses B_1 and B_2 was obtained using a cross-correlation method,[33] and velocity (V) was obtained from τ and the sample thickness (X) according to

$$V = 2\frac{X}{\tau} \qquad (2)$$

Velocity determined from cross-correlation is essentially a group velocity as the entire wave train (containing a broad band of frequencies) is considered in the calculation. It was estimated that the uncertainty in the accuracy of the velocity measurement for the samples in this experiment was $\leq$ 0.4% with the major sources of error being sample and couplant thickness variation, and sample thickness measurement inaccuracy. However, the precision (reproducibility) of the measurement was shown to be on the order of 0.1% or better at a single location on any sample.

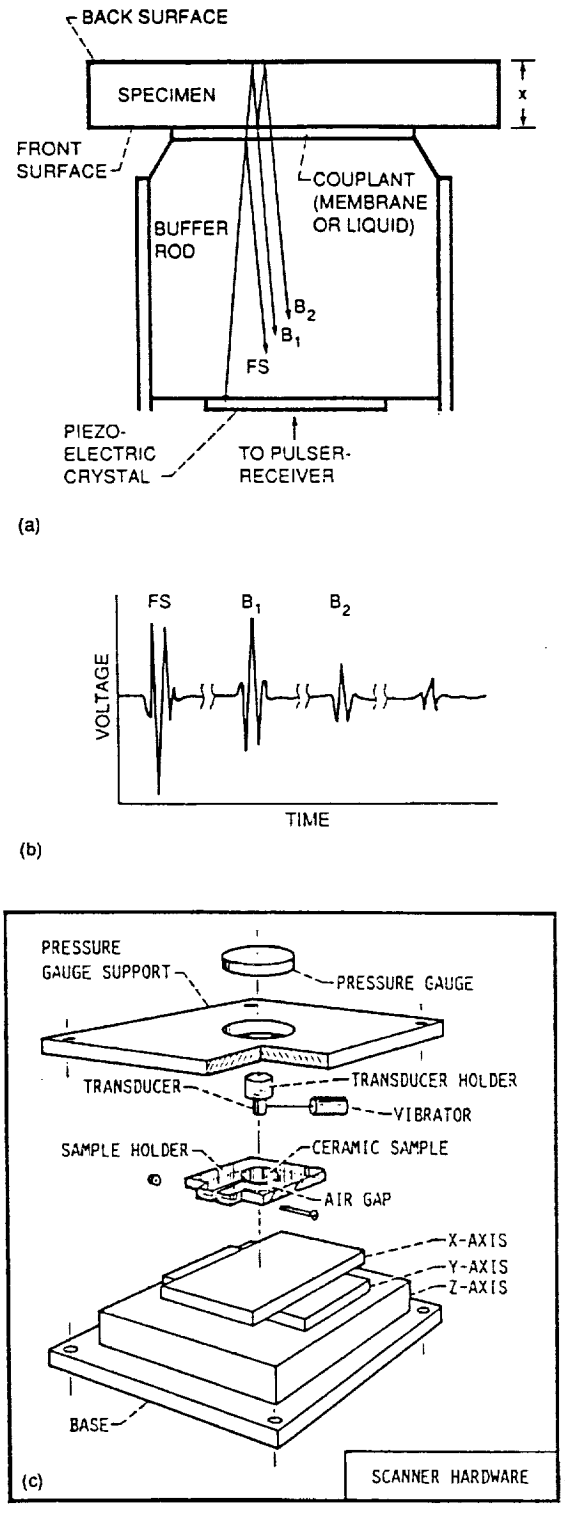

(a) Diagram of transducer/specimen configuration for pulse-echo ultrasonics. FS = Front surface reflection; B_1 = First back surface reflection; B_2 = Second back surface reflection.
(b) Resulting waveforms for pulse-echo contact technique.
(c) Computer-controlled acoustic scanning system.

Fig. 1. – Ultrasonic measurement method.

2. Point Measurement

Point measurements (i.e., measurements at a single location) were made at room temperature on the semicircular sections of samples 1 - 4 using a broadband 5-MHz (center frequency) longitudinal wave transducer connected to a pulser-receiver of 0.01 - 10 MHz bandwidth. The transducer consisted of a critically-damped lead metaniobate element with an active diameter of 1.2 cm bonded to a polystyrene buffer rod 1.6 cm in diameter. A thin (0.04 cm) pliable polymer material attached to the buffer rod allowed ultrasound to be transmitted into the specimen without the need for liquid coupling. Dry coupling avoids contamination and possibly inaccurate results when porous materials absorb a liquid couplant. (However, a 90 percent dense YBCO sample absorbed a negligible amount of couplant.[10]) The sample to be measured for ultrasonic velocity was lightly clamped to the transducer using a small mechanical clamp. The clamp was tightened until stable B_1 and B_2 waveforms of highest signal-to-noise ratio were obtained. 25 measurements were made at the same point without removing the transducer from the sample and an average velocity was obtained. Apparent elastic modulus was calculated from the velocities and bulk densities prior to and after oxidation and reduction assuming ν = 0.27[34](equation (1)). (For all YBCO samples in this study, it was assumed that ν = 0.27. This assumption is not unrealistic for a material undergoing moderate change. Concerning the relationship between ν and pore fraction, for example, most of the limited studies of ν show it decreasing with increasing pore fraction less rapidly than does E.[15])

3. Scanning of Sample 5 Disk

Velocity measurements were obtained at room temperature over an ordered array of points across the surface of the sample 5 machined circular disk by means of an automated scanning technique (figure 1(c)).[10,19] A broadband 10-MHz (center frequency) longitudinal wave transducer (Panametrics, Waltham, MA 02254) connected to the pulser-receiver of 0.01 - 10 MHz bandwidth was used. The transducer had a lead metaniobate crystal with an active diameter of 0.6 cm. The crystal was bonded to a silica glass buffer rod approximately 1.75 cm in diameter. Liquid couplant was necessary between the transducer and sample to allow transmission of ultrasound into the sample and to lubricate the transducer-sample interface so that continuous contact scanning could be performed. A non-aqueous liquid couplant (Dow Corning [Midland, MI 48640] 704 diffusion pump fluid) was used. Contamination from the couplant was assumed minimal due to the high ($\geq$ 90%) density of sample 5.[10]

In preparation for contact scanning, the disk was mounted in a Lucite holder. Before oxidation (table I(b)), after extended oxidation (table I(e)), and after subsequent reduction (table I(c)), a scan was run over the identical 3 mm by 5 mm area near the center of sample 5 with measurements made every 0.5 mm. The contact force on the transducer was maintained at 12 $\pm$ 0.1 lbs. After a set of waveforms was acquired at one point, the x- and or y- positioner table was automatically moved the specified increment to the next point. A vibrator (made from a modified electric scribing tool) was used during this movement to aid in repositioning of transducer and couplant, and to prevent the transducer from jamming on the sample. Additionally, point measurements with this same experimental configuration were made at the scan origin to focus on the change at a single location, similar to the point measurements on samples 1 - 4. Before each scan, the disk was machined so that top and bottom surfaces were flat and parallel ($\pm$ 0.002 mm) while removing a minimum of material (approximately 0.05 - 0.1 mm), and the thickness was measured. The sample was ultrasonically cleaned in anhydrous ethanol for 5 - 10 minutes after each scan to minimize contamination effects during subsequent oxidation / reduction treatments. Typical scan and analysis time for scans consisting of 77 measurements was about 0.5 - 1 hours. Scans were run at least twice to determine reproducibility.

An ultrasonic image was constructed from the velocity values obtained at each scan point. A continuous scale consisting of 256 shades of gray (or color) and linear interpolation between points allowed the display of subtle velocity changes across the sample.[19] The image can be thought of as a two-dimensional projection representing averaged microstructural information for the volume of sample scanned.

D. Microstructural and Compositional Analysis

Pieces of samples 1 - 5 were examined for microstructural and compositional differences prior to and after the oxidation and reduction treatments. Observations of surface macrocracking were made on as-received and treated samples. Bright field optical microscopy was used to obtain porosity and grain

(polarized light) distribution micrographs. Mean grain size was obtained from the optical micrographs of grain distribution using the Heyn-intercept method (ASTM E112-85). Grain size was determined for four orientations (separated by 45°) of the micrograph. Estimated uncertainty in mean grain size was about 20 %. The presence or lack of twinning was noted. Weight percents of Y, Ba, and Cu were measured using inductively-coupled plasma atomic emission spectroscopy (ICP-AES) for which the estimated uncertainty was about 3 to 5 % of the weight percent reading. Estimates of volume percent CuO, a common impurity found in YBCO, were made from the white regions (confirmed by energy-dispersive spectroscopy and electron diffraction to be CuO) in porosity distribution micrographs.

X-ray diffraction (using CuK(α) radiation with a scan rate of 2°/minute) was performed on top, subsurface and bottom surfaces of samples with a computer-controlled diffractometer to determine whether the material was orthorhombic or tetragonal, and whether impurity phases were present in significant quantity. (The YBCO tetragonal and orthorhombic structures can be differentiated in x-ray diffraction by the relative intensities of the peaks at 2θ = 32.5° - 33° as well as by least-squares refinement of the x-ray data to obtain the lattice parameters.[26,35] For the orthorhombic structure, the higher angle peak (103/110) has about twice the intensity of the lower angle peak (013/103) whereas for the tetragonal structure, the (013) peak has about twice the intensity of the (110) peak.) A least-squares refinement procedure was used to determine the unit cell axis lengths. The starting powder was examined for impurities with x-ray diffraction.

Two methods were used to determine oxygen content. The oxygen atom value (7-x) (for $YBa_2Cu_3O_{7-x}$) was determined from the c-axis length using an empirical relationship

$$(7-x) = 76.40 - 5.95(c\text{-}axis) \quad (3)$$

for which the estimated uncertainty in (7-x) was 0.05.[36] Weight percent oxygen was determined on two 50 - 100 mg pieces for each sample using inert gas fusion for which the estimated uncertainty was about 1 % of the weight percent reading.

Since reference 10 determined that ultrasonic velocity variations across a YBCO sample were likely to be caused by spatial variations in volume percent porosity, optical image analysis techniques (described in detail elsewhere[10]) were used in conjuction with ultrasonic scans to determine whether changes in spatial pore distribution (volume percent and size) occurred after oxidation and reduction for sample 5. Measurements were made on 10 randomly-located fields of 0.01 - 0.02 mm^2 area each. The uncertainty in these measurements was around 10%.

E. A.C. Susceptibility

A.c. susceptibility[37] was measured with the Lakeshore Cryotronics (Westerville, OH 43081) Model 7000 susceptometer to examine the normal-to-superconducting transition of the bars cut from samples 1 - 5 prior to and after oxidation and reduction treatments. The normal-to-superconducting transition temperature (T_c) was taken as the onset temperature where the sharp break from 0 m^3/kg in the

real component of susceptibility (χ') occurred. The transition width (ΔT_c) was obtained from temperatures at which 10 and 90 percent of the χ' transition was completed. Average T_c and ΔT_c were obtained from the measurements on the edge- and center-cut bars for each of samples 1 - 4 and from one bar from sample 5. The bars were lightly ground to remove possible contaminants and then ultrasonically cleaned in anhydrous ethanol (and air-dried) before measurements. The specimens, placed into a small nonmagnetic plastic container, were cooled to 4.2 K in zero field. The a.c. field (frequency=100 Hz, magnitude=0.02 Oe) was applied (parallel to the specimen long axis), and the assembly was heated to 100 K through the superconducting-to-normal transition at a rate of 0.7 K / minute. No d.c. field was applied. Approximately one null measurement per degree Kelvin was obtained.[10] Measurements were made prior to and after the oxidation and reduction treatments.

The susceptibilities were external, i.e. demagnetization corrections were not made. (The demagnetization factor is estimated at 0.05 for rectangular bars of the dimensions used in this study.[38] Susceptibility was calculated taking sample volume to be the bulk volume (material + pores). Mass susceptibility was obtained by dividing χ' by bulk density (ρ). The uncertainty in the accuracy of the susceptibility measurement was estimated at 4 % for the bars cut from samples 1 - 5 (due to the uncertainties in the bar dimensions and the accuracy with which voltage is read by the phase sensitive detector). The uncertainty in the accuracy of the temperature measurement was conservatively estimated at 0.5 K.

V. RESULTS AND DISCUSSION

Table II shows the values of properties, compositional characteristics, and structural characteristics of YBCO samples 1 - 5 prior to and after oxidation and reduction. Table III summarizes the changes in properties and lists the structural characteristics after the treatments. Tables II and III first present results for initially-oxidized samples 2, 3, and 4 followed by results for initially-unoxidized samples 1 and 5.

A. General Sample Characterization

1. Composition and Microstructure

ICP-AES results yielded the proper atomic ratio of 1:2:3 for Y:Ba:Cu indicating that elemental stoichiometry for $YBa_2Cu_3O_{7-x}$ remained constant for all samples before and after all oxidations and reductions. CuO impurity volume percent was small (< 1% in most cases) and was not measurably changed after oxidation or reduction. As expected, oxygen content decreased upon reduction and increased upon oxidation for samples 1 - 5 (figure 2). Figure 3 shows weight percent oxygen determined from inert gas fusion versus oxygen atom value (7-x) determined from equation (3) for samples 1 - 5 prior to and after oxidation and reduction. A weaker than expected linear correlation is evident. Equation (3) yielded mean oxygen atom values (7-x) close to those expected for YBCO samples undergoing oxidation / reduction (although standard deviations from the least-squares refinement of the c-axis length (equation (3)) were large in some cases). In most cases, larger mean oxygen weight percents than

Table II. Values of Properties, and Compositional and Structural Characteristics of $YBa_2Cu_3O_{7-x}$

Sample	Peak Sintering Temperature (°C)	Processing	Y:Ba:Cu[a] atomic ratio	Oxygen[b] atom value (7-x)	Weight[c] Percent Oxygen	Volume[d] Percent CuO	T_c (K)[e]	ΔT_c (K)[e]
2	947	oxidized (table I(a))	1:2:3	6.88±0.04	18.0±0.18	< 1	89	2
		reduced (table I(c))	1:2:3	6.68±0.15	17.4±0.17	< 1	0	-
3	954	oxidized (table I(a))	1:2:3	6.93±0.04	18.1±0.27	< 1	88	3
		reduced (table I(c))	1:2:3	6.76±0.15	16.9±0.34	< 1	40	28
4	966	oxidized (table I(a))	1:2:3	6.95±0.04	18.1±0.27	< 1	86	8
		reduced (table I(c))	1:2:3	6.71±0.12	16.4±0.0	< 1	0	-
1	937	unoxidized (table I(b))	1:2:3	6.52±0.17	15.1±0.45	2 - 5	0	4
		oxidized (table I(d))	1:2:3	6.92±0.03	17.7±0.53	2 - 5	89	-
5	976	unoxidized (table I(b))	1:2:3	6.42±0.05	15.0±0.45	< 1	0	-
		oxidized (table I(d))	1:2:3	6.83±0.13	17.2±1.20	< 1	89	7
		extended oxidation (table I(e))	1:2:3	6.90±0.11	17.7±0.11	< 1	78	10
		reduced (table I(c))	1:2:3	6.21±0.07	16.8±0.10	< 1	0	-

[a]Determined from Inductively Coupled Plasma-Atomic Emission Spectroscopy (ICP-AES)[10]

[b]Calculated (mean ± standard deviation) from equation (3) (standard deviation propagated through from standard deviation in c-axis)

[c]Inert gas fusion, mean ± standard deviation for 2 trials (estimated % uncertainty = 1% of reading)

[d]Estimated from white regions in porosity distribution micrographs

[e]Determined from χ' susceptibility response at H_{ac} = 0.02 Oe and f = 100 Hz; uncertainty = 0.5 K; "-" indicates no normal-to-superconducting transition was observed

Table II. Values of Properties, and Compositional and Structural Characteristics of $YBa_2Cu_3O_{7-x}$ Samples - (continued)

Sample	Peak Sintering Temperature (°C)	Processing	Bulk[a] Density (g/cm^3)	Ultrasonic[b] Velocity (cm/ μsec)	Apparent[c] Elastic Modulus x 10^{-6} (psi)	Mean grain[d] Diameter (μm)	Twinning ?	c-axis[e] (Å)	Surface Macrocracking?
2	947	oxidized (table I(a))	4.99	0.374	8.10	2.43	yes	11.684±0.006	no
		reduced (table I(c))	4.85	0.360	7.30	2.49	no	11.717±0.012	yes
3	954	oxidized (table I(a))	5.06	0.420	10.4	2.53	yes	11.675±0.008	no
		reduced (table I(c))	4.86	0.394	8.76	2.78	no	11.705±0.025	yes
4	966	oxidized (table I(a))	5.78	0.497	16.6	4.76	yes	11.673±0.004	yes
		reduced (table I(c))	5.62	0.485	15.3	4.63	no	11.711±0.020	no
1	937	unoxidized (table I(b))	4.37	0.312	4.94	2.12	no	11.745±0.029	no
		oxidized (table I(d))	4.76	0.377	7.85	2.05	not sure	11.679±0.006	?
5	976	unoxidized (table I(b))	5.74	0.498	16.5	4.87	no	11.761±0.009	yes
		oxidized (table I(d))	5.87	0.498	16.9	4.56	yes	11.693±0.022	yes
		extended oxidation (table I(e))	5.85	0.506	17.4	4.91	yes**	11.681±0.019	yes
		reduced (table I(c))	5.72	0.495	16.3	4.71	no	11.797±0.011	yes

**more apparent than after previous oxidation

[a]Bulk density calculated from dry weight and dimensions; uncertainty < 0.5%

[b]Ultrasonic (longitudinal wave) velocity obtained from pulse-echo measurements at 5 MHz (samples 1 - 4) and 10 MHz (sample 5) center frequency; mean of 25 repeated measurements (standard deviation = 0)

[c]Apparent Elastic Modulus calculated from equation (1) assuming $\nu = 0.27$[34]

[d]Mean grain diameter estimated from measurements off of photomicrographs in 4 directions; at least 100 grains sampled (estimated % uncertainty = 20%)

[e]X-ray scans run at 2°/minute with Cu-K α radiation; mean ± standard deviation from least squares refinement

Table III. Changes in Properties and Structural Characteristics of $YBa_2Cu_3O_{7-x}$ Samples After Oxidation and Reduction

Sample	Upon (treatment)	Change in oxygen atom value (7-x)	Change in weight percent oxygen	Superconductor[a] Transformation	Structure[b] Transformation	Percent change in[c] bulk density (ρ)	Percent change in[d] velocity (V)	Percent change in[e] Elastic Modulus (E)
2	reduction	-0.20±0.19	-0.6±0.4	S → NS	Or → T	-2.2	-2.5	-3.1
3	reduction	-0.17±0.19	-1.2±0.6	S → MPS	Or → OII	-3.1	-4.6	-6.3
4	reduction	-0.24±0.16	-1.7±0.3	S → NS	Or → T	-2.5	-2.1	-5.0
1	oxidation	0.40±0.20	2.6±1.0	NS → S	T → Or	6.1	11.6	11.1
5	oxidation	0.41±0.18	2.2±1.7	NS → S	T → Or	2.0	0	1.5
	extended oxidation	0.07±0.24	0.5±1.3	S → PS	Some Or → T'	-0.3	1.4	1.9
	reduction	-0.69±0.18	-0.9±0.2	PS → NS	Or → T	-2.0	-2.0	-4.2

[a]Inferred from change in T_c and ΔT_c:
S = Superconductor
NS = Not Superconducting
PS = Poorer Superconductor
MPS = Much Poorer Superconductor

[b] Deduced from changes in 1) T_c
2) relative intensities of x-ray diffraction peaks at 2 θ = 32.5 - 33°
3) oxygen content
4) unit cell parameters
5) presence of twinning

Or = Orthorhombic (6.8 < (7-x) < 7.0)
OII = Orthorhombic II (6.5 < (7-x) < 6.8)
T = Tetragonal (6.4 < (7-x) < 6.0)
T' = Tetragonal ((7-x) > 7.0)
} for $YBa_2Cu_3O_{7-x}$

[c]percent change in ρ = {100 (ρ_{after} - ρ_{before})/6.381 g/cm^3}; 6.381 g/cm^3 is the theoretical density of $YBa_2Cu_3O_7$

[d]percent change in V = {100 (V_{after} - V_{before})/0.560 cm/ μsec}; 0.560 cm/ μsec is the velocity of fully-dense $YBa_2Cu_3O_7$,[16]

[e]percent change in E = {100 (E_{after} - E_{before})/26.1 x 10^6 psi}; 26.1 x 10^6 psi is the predicted Elastic modulus from mechanical testing of fully-dense $YBa_2Cu_3O_7$[39]

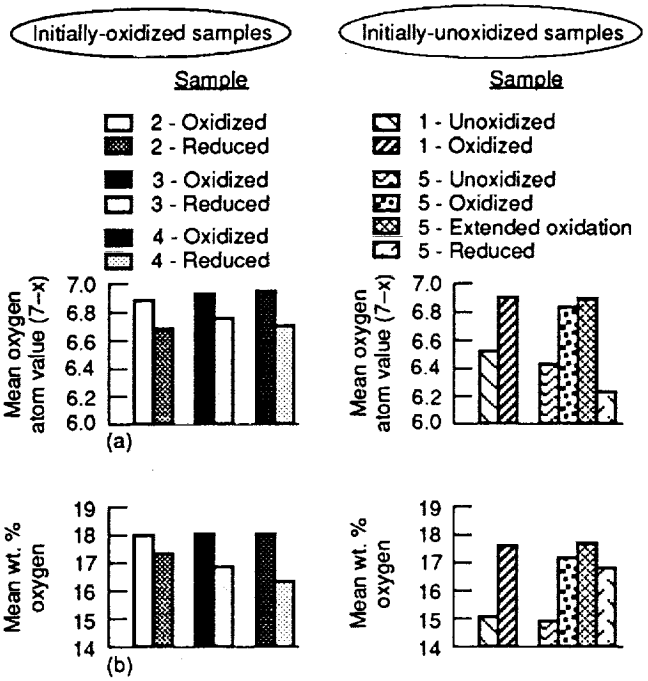

(a) Change in mean oxygen atom value (7–x) (from equation (3)).
(b) Change in mean wt. % oxygen (from inert gas fusion).

Fig. 2. – Effect of oxidation and reduction on oxygen content for YBCO samples 1 - 5.

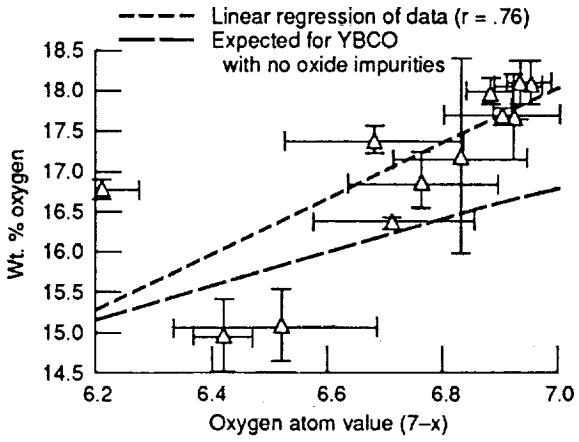

Fig. 3. – Wt. % oxygen versus oxygen atom value (7–x) for $YBa_2Cu_3O_{7-x}$ samples 1 - 5 prior to and after oxidation and reduction. Wt. % oxygen determined from inert gas fusion (mean ± standard deviation for 2 trials). Oxygen atom value determined from equation (3) (mean ± standard deviation; standard deviation propagated through from standard deviation in c-axis).

expected were obtained either confirming the presence of oxide impurity phases or indicating a systematic error in the inert gas fusion technique. The direction and magnitude of mean change appeared reasonable for both oxygen content determination methods.

From x-ray diffraction results, the structure transformed from orthorhombic to tetragonal upon reduction and tetragonal to orthorhombic upon oxidation. The two peaks at 2θ = 32.5° - 33° were seen to reverse in relative intensity (as shown for sample 5 in figure 4), and the unit cell parameters changed as expected upon structure transformation.[26,35] No additional large peaks indicating significant impurity content were apparent in the x-ray diffraction patterns. Twinning, not observed before oxidation and after reduction, was apparent after oxidation (as shown for sample 5 in figure 5).

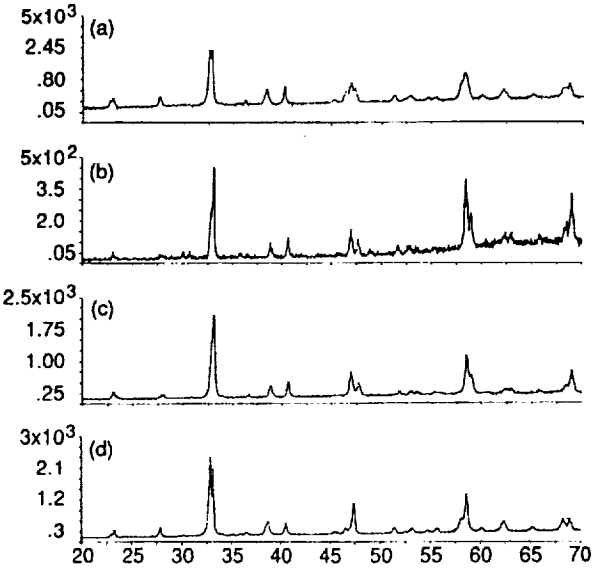

(a) Unoxidized (table I (b)).
(b) Oxidation (table I (d)).
(c) Extended oxidation (table I (e)).
(d) Reduction (table I (c)).

Fig. 4. – X-ray diffraction patterns for sample 5 after oxidation and reduction treatments. Note relative intensities of two peaks at 2θ = 32.5° - 33°.

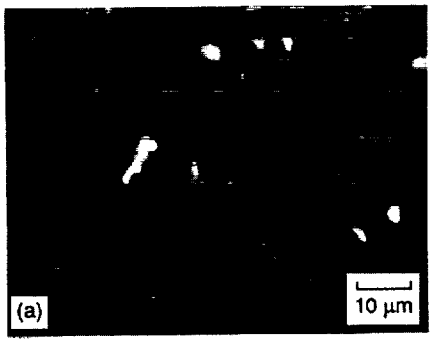

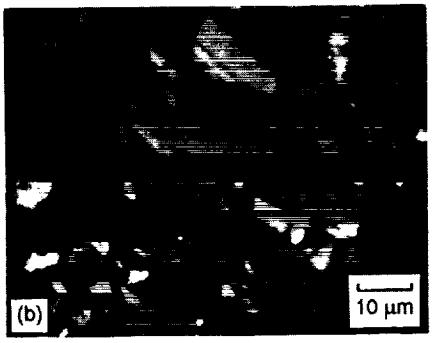

(a) Unoxidized (table I (b)).
(b) Oxidation (table I (d)).

Fig. 5. – Optical micrographs showing grain distribution for sample 5 after oxidation and reduction treatments. Polarized light. Note strong twinning in (c).

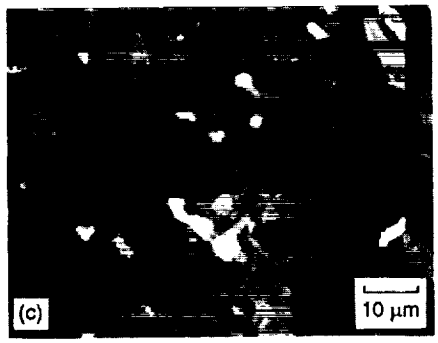

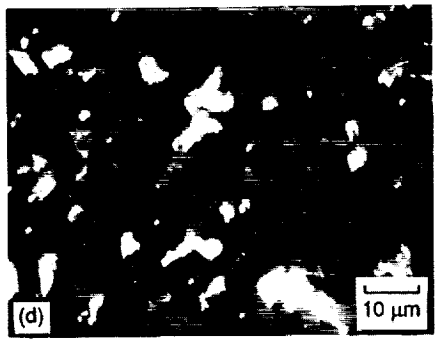

(c) Extended oxidation (table I (e)).
(d) Reduction (table I (c)).

Fig. 5. – Concluded.

Within the uncertainty (±20 %) of the measurement, mean grain size and grain orientation (random) were unchanged after the various treatments. Based on expected unit cell lattice parameter changes, a 1.6 % increase in grain volume (giving < 1% increase in linear dimension) is expected upon reduction for the case where (7-x) decreases from 7 to 6 (excluding any grain growth from further densification). Surface macrocracking (figure 6) was apparent on as-recieved samples 4 and 5, the highest density samples, and was also present after reduction (samples 4 and 5) and oxidations (sample 5). Macrocracks, not apparent on as-received oxidized samples 2 and 3, were seen on the surfaces of the reduced material. Causes of cracking were discussed in the BACKGROUND section. Some macrocracking may also have resulted

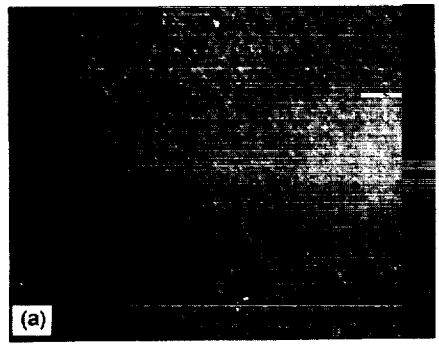

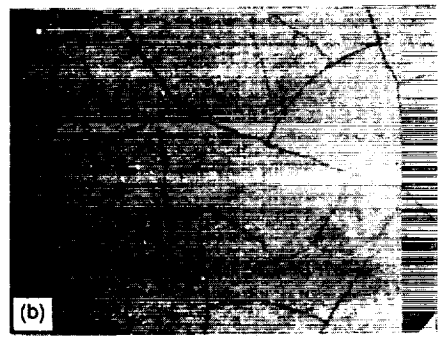

(a) No surface macrocracking for oxidized sample 2.
(b) Surface macrocracking for oxidized sample 5.

Fig. 6. – Photomicrographs of YBCO sample surfaces. Diagonal marks indicate machining grooves.

from machining.

2. Superconductor Behavior

From a.c. susceptibility measurements, the normal-to-superconducting transition was 1) observed for the oxidized samples for which T_c was between 78 and 90 K and 2) not observed for the reduced and unoxidized samples (as shown for sample 5 in figure 7). The increase in oxygen content and appearance of the transition indicate that oxidation times were sufficient to oxygenate the samples to their superconducting (orthorhombic) state regardless of density.

One exception to expected results occurred for sample 3 which had a T_c of about 40 K upon reduction. For this case, it is likely that the orthorhombic material was not fully reduced and the OII phase characterized by $6.5 < (7-x) < 6.8$ and poorer superconducting properties resulted.[6,25,26] The reason why sample 3 was not fully reduced to tetragonal YBCO but samples 2, 4 and 5 appeared to be when undergoing the identical reduction is unknown.

Another exception to expected results occurred for sample 5 upon extended oxidation. Sample 5 after the first oxidation had a T_c of about 89 K; however, further oxidation for an additional 53 hours lowered the transition by about 10 K and increased the transition width (ΔT_c) by about 3 K. This may have resulted from the transformation of some orthorhombic material to the overoxygenated, semiconducting tetragonal T' phase[27,28,29] or from sample contamination in between trials. The large ΔT_c for sample 3 after reduction (ΔT_c = 28 K), and sample 5 after oxidation (ΔT_c = 7 K)

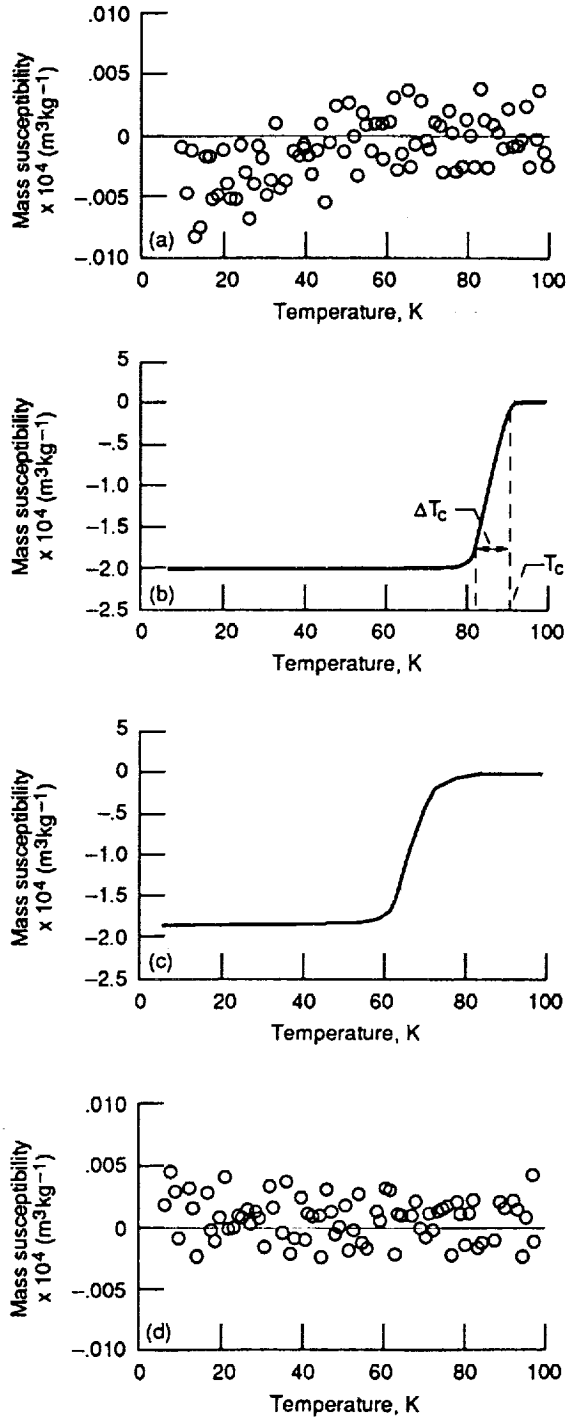

(a) Unoxidized (table I (b)).
(b) Oxidation (table I (d)).
(c) Extended oxidation (table I (e)).
(d) Reduction (table I (c)).

Fig. 7. – A.c. susceptibility versus temperature for sample 5 after oxidation and reduction treatments. H_{ac} = 0.02 Oe. Frequency = 100 Hz.

and extended oxidation (ΔT_c = 10 K), suggests sample inhomogeneity (i.e., the sample may be composed of several YBCO phases having a range of T_c's).[7]

B. Density, Velocity and Elastic Modulus Changes

1. Trends

Figure 8(a) shows the effect of oxidation and reduction on the bulk density of $YBa_2Cu_3O_{7-x}$ samples 1 - 5. In 6 out of 7 cases, bulk density increased (increase in mass and decrease in volume) upon oxidation or decreased (decrease in mass and increase in volume) upon reduction. A density increase is expected upon oxidation; lattice paramater calculations indicate a 4 % increase in crystal density occurs when (7-x) increases from 6 to 7. Sample 1 (the lowest density sample) showed the greatest increase in density (6.1%) upon oxidation, and this magnitude change was beyond that expected for the tetragonal-to-orthorhombic transformation. This was likely due to some sintering resulting in reductions in volume percent porosity because of sample 1's very low initial density.

Figure 8(b) shows the effect of oxidation and reduction on the ultrasonic velocity of YBCO samples 1 - 5. In 6 out of 7 cases, velocity increased upon oxidation and decreased upon reduction. Velocity changes generally showed the same trend as density changes upon the treatments. Sample 1 (the lowest density sample) showed the greatest increase in velocity (11.6%) (accompanying the greatest increase in density (6.1%)) upon oxidation. It is likely that the velocity changes upon oxidation and reduction were influenced most strongly by the density changes[16]

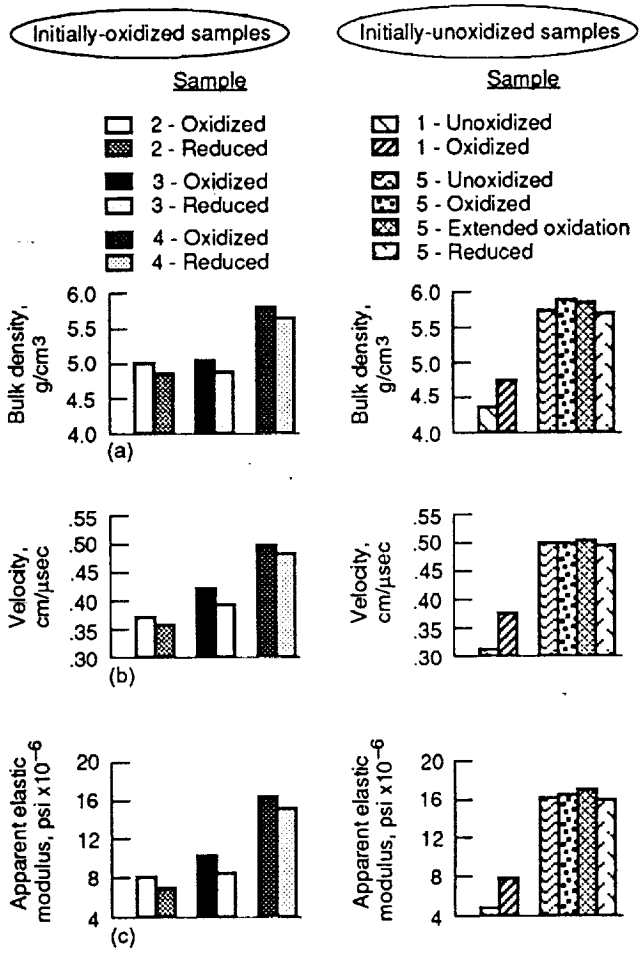

(a) Change in bulk density.
(b) Change in ultrasonic velocity.
(c) Change in apparent elastic modulus.

Fig. 8. – Effect of oxidation and reduction on bulk density, ultrasonic velocity, and apparent elastic modulus for YBCO samples 1 - 5.

accompanying the changes in oxygen content. Therefore, oxygen content changes may be interpreted, at least qualitatively, in terms of density and velocity changes and ultrasonic velocity showed potential for monitoring the oxidation process.

Attempts to quantify the relationship between oxygen content and velocity changes are shown in figure 9. No correlation (correlation coefficient, r = 0.08) is obtained between change in oxygen

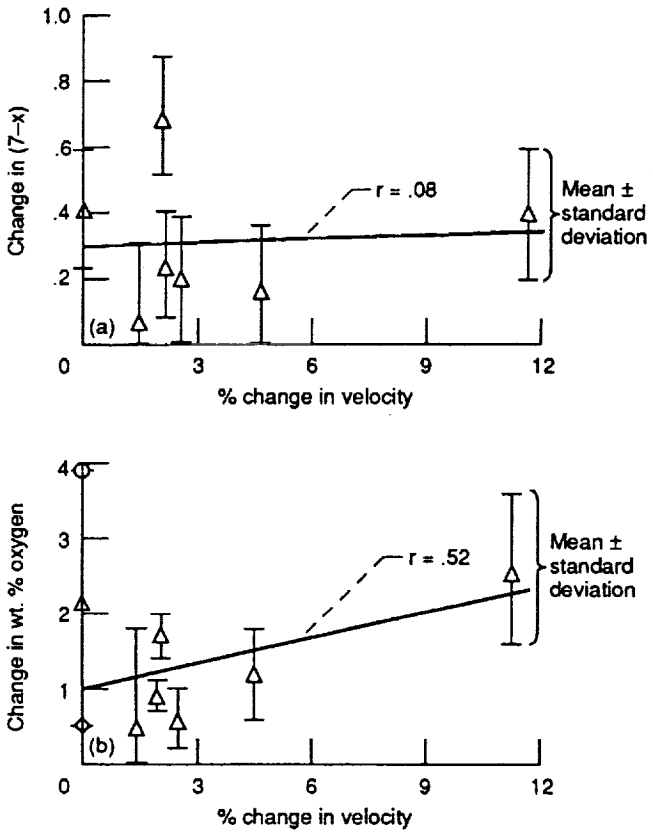

Fig. 9. – Change in oxygen content versus % change in velocity for $YBa_2Cu_3O_{7-x}$ samples 1 - 5 upon oxidation or reduction. Line drawn is from linear regression of data.

atom value (7-x) and percent change in velocity (figure 9(a)) but a weak linear correlation (r = 0.52) is seen between change in weight percent oxygen and percent change in velocity (figure 9(b)). The lack of good quantitative correlation is likely due to 1) changes in crystal structure, grain structure (twinning), oxygen vacancy ordering and crack density affecting velocity in a competing manner to bulk density and 2) insufficient accuracy and precision of the oxygen content determination methods employed (as indicated by the large standard deviations in figure 3).

Figure 8(c) shows the effect of oxidation and reduction on the apparent elastic modulus of YBCO samples 1 - 5. Modulus values ranged from 4.94 x 10^6 psi for unoxidized sample 1 (lowest density sample) to 17.4 x 10^6 psi for sample 5 after extended oxidation. In 7 out of 7 cases for samples 1 - 5, modulus increased upon oxidation and decreased upon reduction, indicating that the structure stiffens with the addition of oxygen. The magnitude of increase ranged from 1.5 to 11.1 percent. Sample 1 (the lowest density sample) showed the greatest increase in modulus upon oxidation. Figure 10 shows the ρV^2 dependence of apparent elastic modulus.

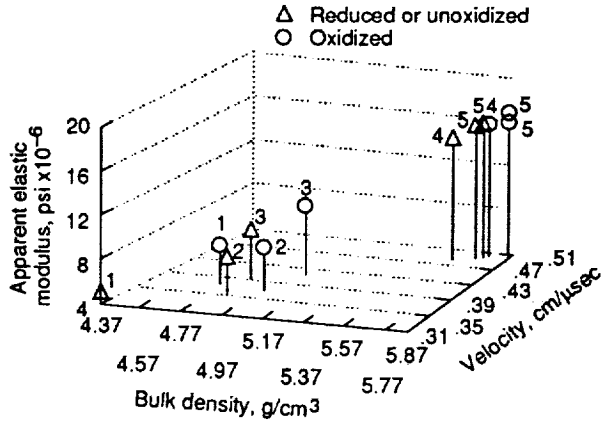

Fig. 10. – Apparent elastic modulus as a function of bulk density and ultrasonic velocity for YBCO samples 1 - 5. Modulus calculated from equation 1 assuming ν = 0.27 (ref. 34). Sample number indicated above symbol.

2. Unexpected Results

Several exceptions to expected velocity and density results occurred. First, upon the first oxidation of sample 5, velocity remained essentially constant even though oxygen atom value (7-x) increased substantially (0.41 ± 0.18) and density increased moderately (2.0%). Then, upon extended oxidation of sample 5, velocity increased (1.4%) but density remained unchanged or

decreased slightly. As previously noted, the relatively large ΔT_c for sample 5 after oxidation (ΔT_c = 7 K) and extended oxidation (ΔT_c = 10 K) suggest sample inhomogeneity (the presence of multiple phases) which might have contributed in some manner to the unexpected results.[7] Additionally, the microstructural changes upon oxidation may have affected velocity, perhaps in a competing manner to density and oxygen content changes.

Further unexpected results involved the relationship between velocity and bulk density for samples 2 and 3. Samples 2 and 3 in their initial oxidized state had very similar densities but largely different velocities (about 8% difference, normalized to the velocity of 0.560 cm/μsec for fully-dense YBCO) indicating some structural and/or compositional difference between the samples. However, no significant differences in Y:Ba:Cu atomic ratio, oxygen content, CuO impurity volume percent, grain diameter, pore morphology, twinning, unit cell dimensions, or surface macrocracking were noted for the two samples. It is possible that differences in the amount of internal microcracking or amounts of other impurity phases caused the velocity difference between the samples.

C. Elastic Modulus of Fully-Dense Materials

Figure 11(a) shows a scatter plot of longitudinal wave velocity versus percent porosity for orthorhombic YBCO obtained from the velocity and density data of all oxidized samples. (To calculate percent porosity, fully-dense orthorhombic $YBa_2Cu_3O_{7-x}$ was assumed to have (7-x) = 7, a unit cell volume of 173.30 Å^3, and a molecular weight of 666 g yielding a theoretical density of 6.381 g/cm^3 for $YBa_2Cu_3O_7$.[26]) Figure 11(b) shows a scatter plot of longitudinal wave velocity versus percent porosity for tetragonal YBCO obtained from the velocity and density data of reduced samples 2, 4 and 5 and unoxidized samples 1 and 5. (To calculate percent porosity, fully-dense tetragonal $YBa_2Cu_3O_{7-x}$ was assumed to have (7-x) = 6.4, a unit cell volume of 176.20 Å^3, and a molecular weight of 656.4 g yielding a theoretical density of 6.188 g/cm^3 for $YBa_2Cu_3O_{6.4}$.[35]) Linear regression analyis[16] yielded similar intercepts (which represent the velocities for

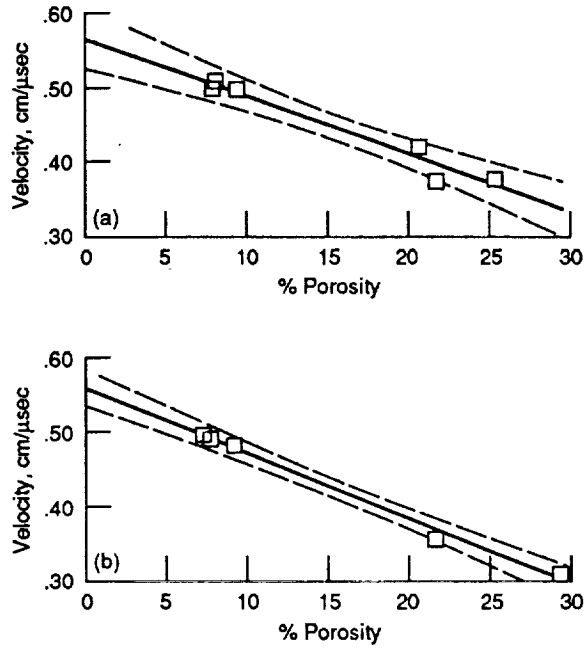

(a) Orthorhombic $YBa_2Cu_3O_{7-x}$ samples. Velocity (cm/μsec) = –0.008 x % porosity + 0.566; correlation coefficient = –0.977; assume theoretical density of 6.381 g/cm3 ((7 – x) = 7) for % porosity calculation.
(b) Tetragonal $YB_2Cu_3O_{7-x}$ samples. Velocity (cm/μsec) = –0.009 x % porosity + 0.561; correlation coefficient = –0.996; assume theoretical density of 6.188 g/cm3 ((7 – x) = 6.4) for % porosity calculation.

Fig. 11. – Longitudinal velocity versus % porosity for orthorhombic and tetragonal YBCO samples. Dashed lines show 95% confidence interval for mean predicted velocity values.

fully-dense material) of 0.566 cm/μsec for orthorhombic YBCO and 0.561 cm/μsec for tetragonal YBCO. Elastic modulus calculated from equation (1) for fully-dense materials yielded similar values of 22.6 x 10^6 psi for tetragonal YBCO and 23.6 x 10^6 psi for orthorhombic YBCO. The latter value for orthorhombic YBCO agrees within 10% of that predicted from extrapolation of mechanical test data (26.1 x 10^6 psi).[39]

D. Global Microstructure of Sample 5

1. Ultrasonic Velocity Images

Figure 12 shows the ultrasonic velocity images obtained over the 3 mm by 5 mm region near the center of sample 5 prior to and after oxidation and reduction treatments. Total velocity variation over the scan region was less than 1% for each case. A similar pattern of velocity variation was evident with the highest (lower portion of image) and lowest (upper portion of image) velocity regions remaining intact after the treatments. The most significant change in velocity magnitude occurred upon reduction where the total velocity variation doubled from 0.4% to 0.8%. The mean, minimum, and maximum velocity values for the 77 measurements used to form each image changed after oxidation and reduction in an almost identical fashion to that for the point measurements made at the scan origin (tables II and III). The fact that the velocity changed at each measurement location upon treatment, and yet the velocity variation pattern remained nearly constant, indicated that the material changed upon oxidation and reduction but in a uniform manner from point to point within the scan region. Higher ($\geq$ 90 % of theoretical) density YBCO samples such as sample 5 are thought to be subject to oxygen content nonuniformity due to pore closure and subsequent oxidation by slow bulk diffusion.[40] The unchanging velocity pattern suggests that the extended oxidation time of 53 hours at 600 °C is sufficient for uniform oxygenation of such high density samples, and that as a result, spatial variations in superconductor properties may not exist as they did for 90 % dense YBCO samples undergoing post-sintering oxidations of around 16 hours at 300 - 600 °C.[41] The unchanging velocity pattern also may indicate that *changes in* surface and bulk crack density occurring upon oxidation and reduction across this sample location were insignificant or, in any case, had a negligible effect on velocity.

2. Spatial Pore Distribution

Figure 13 shows representative pore size distribution photomicrographs of polished sections of sample 5 after oxidation and reduction treatments. Mean percent porosity and mean pore length from optical image analysis of random areas within cross-sections yielded similar values (about 9 - 10 percent porosity and 1.6 - 1.9 μm mean pore length) within the uncertainty of the measurement after oxidation and reduction. This supports the velocity image results indicating that no significant global changes in microstructure occurred during the treatments. Had spatial pore distribution been significantly altered, it is believed that the velocity image would have changed much more drastically as was shown previously by reference 42 for step-sintered SiC samples. Density

ORIGINAL PAGE
BLACK AND WHITE PHOTOGRAPH

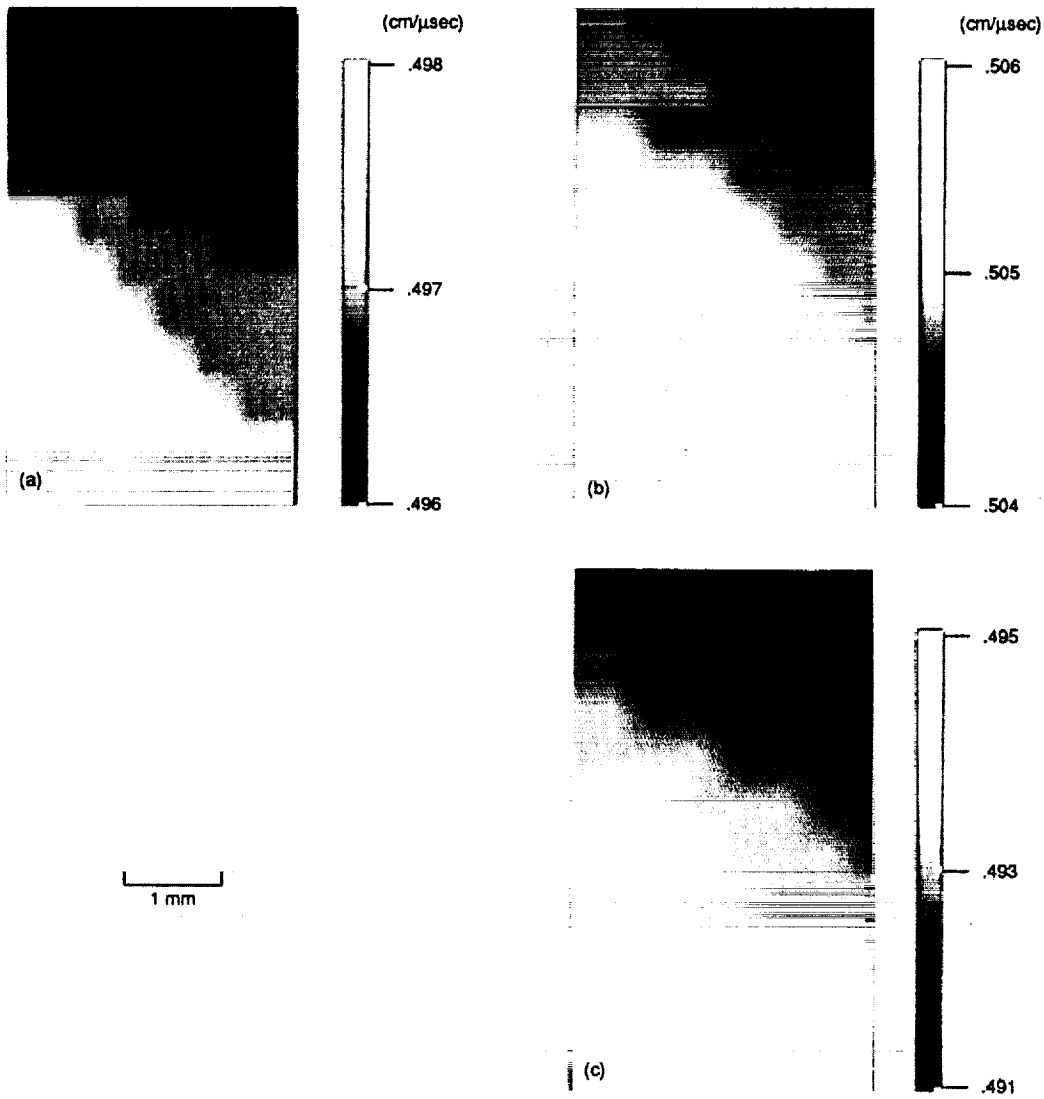

(a) Unoxidized (table I (b)).
(b) Extended oxidation (table I (e)).
(c) Reduction (table I (c)).

Fig. 12. – Ultrasonic velocity images of sample 5 after oxidation and reduction treatments. Ultrasonic broadband transducer center frequency = 10 MHz. Scan was run over 3 mm by 5 mm region of sample with measurements made every 0.5 mm. Mean, minimum and maximum values change but global pattern stays approximately the same after treatments.

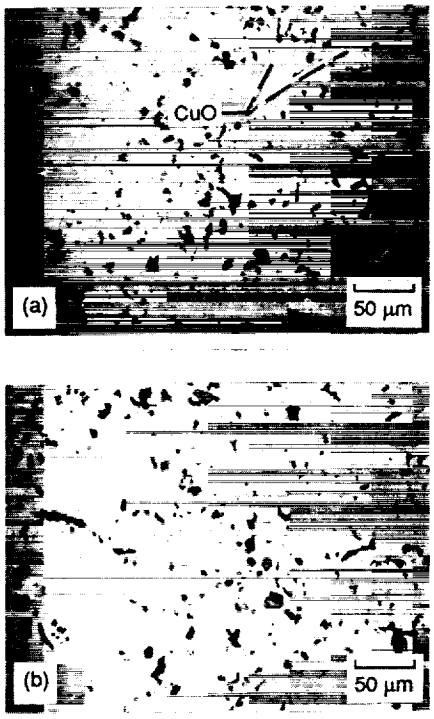

(a) Unoxidized (table I (b)). Mean % porosity = 9.4 %; mean pore length = 1.89 μm.
(b) Oxidation (table I (d)). Mean % porosity = 9.7 %; mean pore length = 1.60 μm.

Fig. 13. – Optical micrographs of porosity distribution for sample 5 after oxidation and reduction treatments. Pore distribution (size and fraction) appears unaffected by treatments.

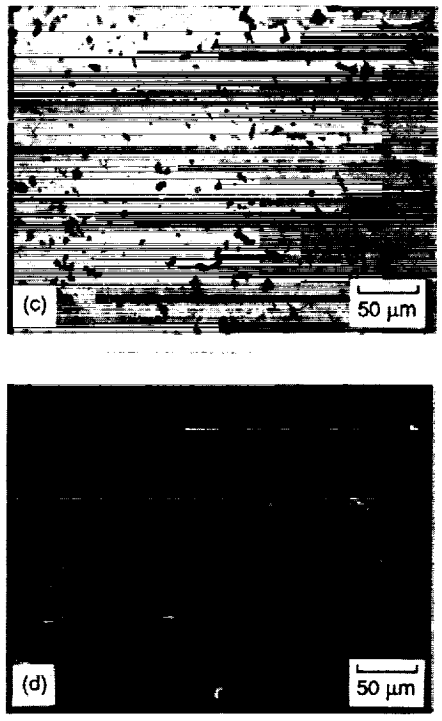

(c) Extended oxidation (table I (e)). Mean % porosity = 8.7 %; mean pore length = 1.69 μm.
(d) Reduction (table I (c)). Mean % porosity = 9.6 %; mean pore length = 1.73 μm.

Fig. 13. – Concluded.

and thus velocity changes were likely to occur as a result of the mass and volume changes taking place during the tetragonal-to-orthorhombic transformation in YBCO, rather than from sintering densification since little sintering is likely to occur at the oxidation/reduction peak temperature (around 800 °C). (However, sample 1 did experience an increase in density beyond that expected for the tetragonal-to-orthorhombic transformation possibly due to its low initial density.)

F. Further Discussion

1. Elastic Modulus Calculation

In theory, elastic moduli are most accurately calculated from phase velocities, i.e., velocity at one specific frequency, since the elasticity of a material may depend on the loading rate.[11] As previously mentioned, velocity determined from cross-correlation is essentially a group velocity as the entire wave train (containing a broad band of frequencies) is considered in the calculation. Group and phase velocity will be essentially equal over the frequency bandwidth investigated if dispersion (velocity varying with frequency) due to the material itself and sample geometry are negligible.[11,12,32] Phase velocity was determined for YBCO samples 1 -

5 using the method of reference 19 and was seen to be essentially constant over the frequency bandwidth of the fourier-transformed B_1 and B_2 waveforms (measured between points at 0.707 times the maximum amplitude) and similar in magnitude (within about 1 percent) to cross-correlation velocity values (figure 14). Thus, the modulus values obtained from cross-correlation velocity measurements were deemed to be sufficiently accurate.

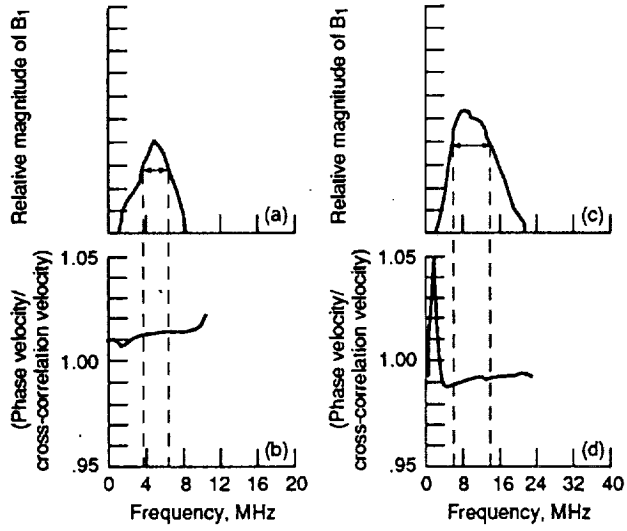

(a) Frequency spectrum of first back-surface reflected pulse (B_1) in sample 1 before oxidation. Broadband transducer of nominal center frequency = 5 MHz. Arrow indicates bandwidth (~4-7 MHz).
(b) (Phase velocity/cross-correlation velocity) for sample 1 before oxidation.
(c) Frequency spectrum of first back-surface reflected pulse (B_1) in sample 5 after reduction. Broadband transducer of nominal center frequency = 10 MHz. Arrow indicates bandwidth (~6-15 MHz).
(d) (Phase velocity/cross-correlation velocity) for sample 5 after reduction.

Fig. 14. – Comparison of cross-correlation and phase velocities over valid frequency bandwidth for 2 representative YBCO samples.

2. Further Experiments

For more exact correlations relating velocity with oxygen content in YBCO, it would be desirable to examine single crystals with precisely-controlled amounts of oxygen (possibly covering a range of $6 \leq (7-x) \leq 7$ with $\Delta x = 0.1$). In conjuntion with experiments on polycrystalline YBCO, this would also allow the determination of bulk solid effects as well. However, ultrasonic experiments on YBCO single crystals are extremely difficult due to the small size of the crystals (0.2 mm by 0.2 mm x 0.1 mm).[43]

In this study, a small (3 mm by 5 mm) region of a YBCO sample was ultrasonically scanned to examine global microstructural change. A future experiment might be desirable which incorporates a scan over an entire YBCO disk surface (eg. 25 mm diameter) to determine if oxidation and reduction processes result in uniform material change over an entire sample.

VI. CONCLUSIONS

Ultrasonic velocity measurement techniques were used to evaluate the effects of oxidation and reduction on the elastic properties, global microstructure and oxygen content of the $YBa_2Cu_3O_{7-x}$ (YBCO) ceramic superconductor for samples ranging from 70 to 90 percent of theoretical density. Bulk density, velocity, and elastic modulus generally increased with increasing oxygen content upon oxidation, and this behavior was reversible. It is likely that the velocity changes upon oxidation and reduction were influenced most strongly by the density changes accompanying the changes in oxygen content. Thus oxygen content changes may be interpreted, at least qualitatively, in terms of density and velocity changes, and ultrasonic velocity showed potential for monitoring the oxidation process. Quantitative correlations between velocity and oxygen content changes were weak probably due to 1) changes in crystal structure, grain structure

(twinning), oxygen vacancy ordering, and crack density affecting velocity in a competing manner to bulk density and 2) insufficient accuracy and precision of the oxygen content determination methods employed. Elastic modulus predicted from velocity and density values for fully-dense materials yielded similar values of 22.6 x 10^6 psi for tetragonal YBCO and 23.6 x 10^6 psi for orthorhombic YBCO.

Velocity images over a 3 mm by 5 mm area of a 25 mm diameter 90% dense YBCO sample were similar after oxidation and reduction treatments, although the velocity value at any given point on the sample was changed following the treatments. The unchanging velocity pattern 1) correlated with destructive measurements showing that the spatial pore distribution (fraction and size) was not measurably altered after the treatments and 2) suggested that the extended oxidation time of 53 hours was sufficient for uniform oxygenation of such high ($\geq$ 90 % of theoretical) density samples.

Changes in superconducting behavior, grain structure and crystal structure were observed to be consistent with oxidation and reduction treatments.

ACKNOWLEDGEMENTS

The authors wish to thank Robert E. Miller of W.R. Grace and Company for his help in sample preparation and the technical support staff at NASA - Lewis Research Center for sample analyses.

REFERENCES

1. J.G. Bednorz and K.A. Muller, "Possible High T_c Superconductivity in The Ba-La-Cu-O System," Z. Phys. B. 64[9] 189-193 (1986).

2. P.H. Hor, R.L. Meng, L. Gao, Z.J. Huang, Y.Q. Wang, K. Forster, J. Vassilious, C.W. Chu, M.K. Wu, J.R. Ashburn and C.J. Torng, "High Pressure Study of The New Y-Ba-Cu-O Superconducting Compound System," Phys. Rev. Lett. 58[9] 911 - 912 (1987).

3. H. Maeda, Y. Tanaka, M. Fukutomi, T. Asano, "A New High-T_c Oxide Superconductor Without a Rare Earth Element," Jpn. J. Appl. Phys. Lett. 27[2] L209 -L210 (1988).

4. Z.Z. Sheng and A.M. Hermann, "Superconductivity in The Rare-Earth Free Tl-Ba-Cu-O System Above Liquid Nitrogen Temperatures," Nature 332[6159] 55 - 58 (1988).

5. R. Beyers, G. Lim, E.M. Engler, V.Y. Lee, M.L. Ramirez, R.J. Savoy and R.D. Jacowitz, "Annealing Treatment Effects on Structure and Superconductivity in $Y_1Ba_2Cu_3O_{9-x}$," Appl. Phys. Lett. 51[8] 614 - 616 (1987).

6. R. Beyers, B.T. Ahn, G. Gorman, V.Y. Lee, S.S.P. Parkin, M.L. Ramirez, K.P. Roche, J.E. Vazquez, T.M. Gur and R.A. Huggins, "Ordered Oxygen Arrangements in $Y_1Ba_2Cu_3O_{7-x}$," High Temperature Superconductors, J.D. Jorgensen, et al., eds., Mat. Res. Soc. Symp. Proc. Vol.156, 1989, pp.77 - 82.

7. D.R. Clarke, T.M. Shaw, and D. Dimos, "Issues in The Processing of Cuprate Ceramic Superconductors," J. Amer. Ceram. Soc. 72[7] 1103 - 1113 (1989).

8. M.F. Yan, R.L. Barns, H.M. O'Bryan Jr., P.K. Gallagher, R.C. Sherwood and S. Jin, "Water

Interaction with the superconducting $YBa_2Cu_3O_{7-x}$ phase," Appl. Phys. Lett. 51[7] 532 - 534 (1987).

9. J. W. Ekin, "Mechanical Properties and Strain Effects in Superconductors," Superconductor Materials Science, Plenum Press, 1981, pp.455 - 510.

10. D.J. Roth, "Property and Microstructural Nonuniformity in the Yttrium-Barium-Copper-Oxide Superconductor Determined from Electrical, Magnetic, and Ultrasonic Measurements," Ph. D. Thesis. Case Western Reserve University, 1991, (also NASA TM-103732).

11. L.C. Lynnworth, Ultrasonic Measurements For Process Control: Theory, Techniques, Applications, Academic Press, 1989.

12. J. Szilard, "Physical Principles of Ultrasonic Testing," Ultrasonic Testing, J. Szilard, ed., Wiley, 1982, pp.1-23 and 557-558.

13. R. Truell, C. Elbaum and B.B. Chick, Ultrasonic Methods in Solid State Physics, Academic Press, 1969, pp.77 - 78 and 159 - 179.

14. G.A. Alers, "The Measurement of Very Small Sound Velocity Changes and Their Use in The Study of Solids," Physical Acoustics, Vol. IV, Part A, W.P. Mason, ed., Academic Press, 1966, pp.277 - 297.

15. R.W. Rice, "Microstructure Dependence of Mechanical Behavior of Ceramics," Properties of Microstructure, R.K. MacCrone, ed., Academic Press, 1977, pp.199 - 381.

16. D.J. Roth, D.B. Stang, S.M. Swickard and M.R. DeGuire, "Review and Statistical Analysis Analysis of The Ultrasonic Velocity Method For Estimating The Porosity Fraction in Polycrystalline Materials," NASA TM-102501, 1990.

17. H. Hsu and H. Conrad, "Ultrasonic Wave Velocity Measurements on Titanium-Oxygen Alloys," Scr. Metall. 5[10] 905 - 908 (1971).

18. S.R. Buxbaum and R.E. Green Jr., "Ultrasonic Characterization of Titanium 6211 Weldments," Nondestructive Methods For Material Property Determination, C.O. Ruud and R.E. Green, Jr., eds., Plenum Press, 1984, pp.271 - 287.

19. E.R. Generazio, D.J. Roth and G.Y. Baaklini, "Acoustic Imaging of Subtle Porosity Porosity Variations in Ceramics," Mater. Eval. 46[9] 1338 - 1343 (1988).

20. D.C. Kunnerth, K.L. Telschow and J.B. Walter, "Characterization of Porosity Distributions in Advanced Ceramics: A Comparison of Ultrasonic Methods," Mater. Eval. 47[5] 571 - 575 (1989).

21. J.J. Gruber, J.M. Smith and R.H. Brockelman, "Ultrasonic Velocity C-Scans for Ceramic and Composite Material Characterization," Mater. Eval. 46[1] 90 - 96 (1988).

22. N.N. Hsu, T.M. Proctor Jr. and G.V. Blessing, "An Analytical Approach to Reference Samples For Ultrasonic Residual Stress Measurement," J. Testing and Evaluation. 10[5] 230 - 234 (1982).

23. G.S. Kino, D.M. Barnett, N. Grayelli, G. Herrman, J.B. Hunter, D.B. Ilic, G.C. Johnson, R.B. King, M.P. Scott and J.C. Shyne, "Acoustic Measurements of Stress Fields and Microstructure," J. Nondestructive Eval. 1[1] 67 - 77 (1980).

24. Y. Iye, "Anisotropic Superconducting and Normal State Transport Properties of HTSC Single Crystals," Studies of High Temperature Superconductors, Vol. 2, A. Narlikar, ed., Nova Science, 1989, pp.199 - 223.

25. I. Chen, S.J. Keating, C.Y. Keating, X. Wu, J. Xu, P.E. Reyes-Morel and T.Y. Tien, "Structural Behavior and Superconductivity of $YBa_2Cu_3O_x$," Sol. St. Comm. 63[11] 997 - 1001 (1987).

26. W. Wong-Ng, H.F. McMurdie, B. Paretzkin, C.R. Hubbard and A.L. Dragoo, "Standard X-Ray Diffraction Powder Patterns of Fourteen Ceramic Phases," Powder Diffraction. 3[2] 113 - 121 (1988).

27. K.W. Lay, "The Formation of Yttrium Barium Cuprate at Low Temperatures," General Electric Corporate Research and Development Technical Information Series, Report #88CRD144 (1988).

28. Y. Nakazawa, M. Ishikawa, T. Takabatake, K. Koga and K. Terakura, "Characterization of Metamorphic Phases of $Ba_2YCu_3O_{9-x}$," Jap. J. Appl. Phys. Lett. 26[5] L796 - L798 (1987).

29. C.C. Torardi, E.M. McCarron, M.A. Subramanian, H.S. Horowitz, J.B. Michel and A.W. Sleight, "Structure - Property Relationships For $RBa_2Cu_3O_x$ Phases," Chemistry Of High-Temperature Superconductors, D.L. Nelson, M.S. Whittingham and T.F. George, eds. ACS Symposium Series, 351, American Chemical Society, 1987, pp.152 - 163.

30. P.K. Gallagher, H.M. O'Bryan, S.A. Sunshine and D.W. Murphy, "Oxygen Stoichiometry in $YBa_2Cu_3O_x$," Mater. Res. Bull. 22[7] 995 - 1006 (1987).

31. H.A. Hoff and C.S. Pande, "Twins in High T_c Superconductors," Studies of High Temperature Superconductors, Vol. 3, A. Narlikar, ed., Nova Science, 1989, pp.333 - 368.

32. M.A. Breazeale, J.H. Contrell and J.S. Heymann, "Ultrasonic Wave Velocity and Attenuation Measurements," Methods of Experimental Physics, Ultrasonics, Vol. 19, P.D. Edmonds, ed., Academic Press, 1981, pp.67 - 135.

33. D.R. Hull, H.E. Kautz and A. Vary, "Measurement of Ultrasonic Velocity Using Phase-slope and Cross-Correlation Methods," Mater. Eval. 43[11] 1455 - 1460 (1985).

34. J.E. Blendell, C.K. Chiang, D.C. Cranmer, S.W. Freiman, E.R. Fuller Jr., E. Drescher-Krasicka, W.L. Johnson, H.M. Ledbetter, L.H. Bennet, L.J. Swartzendriber, R.B. Marinenko, R.L. Myklebust, D.S. Bright and D.E. Newbury, "Processing-Property Relations for $YBa_2Cu_3O_{(7-x)}$ High-T_c Superconductors," Adv. Ceram. Mater. 2[3B] 512 - 529 (1987).

35. W. Wong-Ng, H.F. McMurdie, B. Paretzkin, Y. Zhang, K.L. Davis, C.R. Hubbard, A.L. Dragoo and J.M. Stewart, "Standard X-Ray Diffraction Powder Patterns of Sixteen Ceramic Phases," Powder Diffraction 2[3] 191 - 201 (1987).

36. T. Wolf, I. Apfelstedt, W. Goldacker, H. Kupfer and R. Flukiger, "Preparation and Characterization of Isotropic and Textured $YBa_2Cu_3O_{7-x}$ With High Density and Low Residual Resistivity," Physica C. 153 - 155 351 - 352 (1988).

37. M. Couach, A.F. Khoder and F. Monnier, "Study of Superconductors by A.C. Susceptibility," Cryogenics, 25[12] 695 - 699 (1985).

38. B.D. Cullity, Introduction to Magnetic Materials, Addison - Wesley, 1972, p.618.

39. N.McN. Alford, J.D. Birchall, W.J. Clegg, M.A. Harmer and K. Kendall, "Physical and Mechanical Properties of $YBa_2Cu_3O_{(7-x)}$ Superconductors," J. Mater. Sci. 23:[3] 761 - 768 (1988).

40. N.McN. Alford, W.J. Clegg, M.A. Harmer, J.D. Birchall, K. Kendall and D.H. Jones, "The Effect of Density on Critical Current and Oxygen Stoichiometry of $YBa_2Cu_3O_x$ Superconductors," Nature 332[6159] 58 - 59 (1988).

41. D.J. Roth, M.R. DeGuire, L.E. Dolhert and A.F. Hepp, "Spatial Variations in A.C. Susceptibility and Microstructure for the $YBa_2Cu_3O_{7-x}$ Superconductor and Their Correlation with Room-Temperature Ultrasonic Measurements," 1991, NASA TM-103787, to be published in J. Mater. Res., October, 1991.

42. E.R. Generazio, D.J. Roth, and D.B. Stang, "Ultrasonic Imaging of Porosity Variations Produced During Sintering," J. Am. Ceram. Soc. 72[7] 1282 - 1285 (1989).

43. D.L. Kaiser, F.W. Gayle, R.S. Roth and L.J. Swartzendruber, "Thermomechanical detwinning of superconducting $YBa_2Cu_3O_{7-x}$ single crystals," J. Mater. Res. 4[4] 745 - 747 (1989).

NASA
National Aeronautics and Space Administration

Report Documentation Page

1. Report No.	2. Government Accession No.	3. Recipient's Catalog No.
NASA TM-104529		

4. Title and Subtitle
Ultrasonic Evaluation of Oxidation and Reduction Effects on the Elastic Behavior and Global Microstructure of $YBa_2Cu_3O_{7-x}$

5. Report Date
July 1991

6. Performing Organization Code

7. Author(s)
Don J. Roth, Mark R. DeGuire, and Leonard E.Dolhert

8. Performing Organization Report No.
E-6282

10. Work Unit No.
506-43-11

9. Performing Organization Name and Address
National Aeronautics and Space Administration
Lewis Research Center
Cleveland, Ohio 44135-3191

11. Contract or Grant No.

13. Type of Report and Period Covered
Technical Memorandum

12. Sponsoring Agency Name and Address
National Aeronautics and Space Administration
Washington, D.C. 20546-0001

14. Sponsoring Agency Code

15. Supplementary Notes
Don J. Roth, NASA Lewis Research Center; Mark R. DeGuire, Case Western Reserve University, Dept. Materials Science and Engineering, Cleveland, Ohio 44106; Leonard E. Dolhert, W.R. Grace & Company, Research Division, Columbia, Maryland 21044. Responsible person, Don J. Roth, (216) 433-6017.

16. Abstract
Ultrasonic velocity measurement techniques were used to evaluate the effects of oxidation and reduction on the elastic properties, global microstructure and oxygen content of the $YBa_2Cu_3O_{7-x}$ ceramic superconductor for samples ranging from 70 to 90 percent of theoretical density. Bulk density, velocity and elastic modulus generally increased with increasing oxygen content upon oxidation, and this behavior was reversible. Velocity image patterns were similar after oxidation and reduction treatments for a 90 percent dense sample, although the velocity value at any given point on the sample was changed following the treatments. The unchanging pattern correlated with destructive measurements showing that the spatial pore distribution (fraction and size) was not measurably altered after the treatments. Changes in superconducting behavior, crystal structure, and grain structure were observed consistent with changes in oxygen content.

17. Key Words (Suggested by Author(s))
Ultrasonics; Velocity; Modulus; Oxygen; Microstructure; Density; Nondestructive evaluation; Ceramics; Superconductors; Yttrium-barium-copper-oxide

18. Distribution Statement
Unclassified - Unlimited
Subject Category 38

19. Security Classif. (of the report)	20. Security Classif. (of this page)	21. No. of pages	22. Price*
Unclassified	Unclassified	28	A03

NASA FORM 1626 OCT 86

*For sale by the National Technical Information Service, Springfield, Virginia 22161